4.6 Target Selection

Given that laser and heavy ions can be built to deliver MJ of pulses onto small foci, a key element in an inertial fusion energy (IFE) reactor is the design of the DT target. The IFE driver designs are dictated, in large part, by the target configuration as well as the requirements set forth by the target designers for achieving a uniform DT target implosion. Depending upon the stringency of DT target irradiation requirements in terms of uniformity of illumination (in the case of the laser driver) or in the beam diameters on target (in the case of the heavy ion driver), the requirements placed on the drivers may be sufficiently demanding that the resulting driver costs would be unaffordable. Thus it is of vital importance that the target irradiation requirements for both Prometheus-L and Prometheus-H be well understood. The following section describes the types of DT targets and target irradiation requirements currently being considered for both laser-driven and heavy ion-driven IFE reactors.

4.6.1 Laser Driver Target - The Target Working Group (TWG) has provided the study team with prescriptions for target illumination for both direct and indirect laser-driven targets.[1] At the present time, owing to the higher target gain, we selected the direct-drive IFE laser target was selected as the baseline. Therefore efforts were concentrated on the direct-drive laser target illumination problem. A schematic of this target is shown in Figure 4.6.1-1.

The direct-drive laser target consists of a polystyrene shell surrounding a layer of DT ice and a central region of DT vapor. As an example, for a driver energy of 1.6 MJ, the radius of such a target would be 0.2 cm.

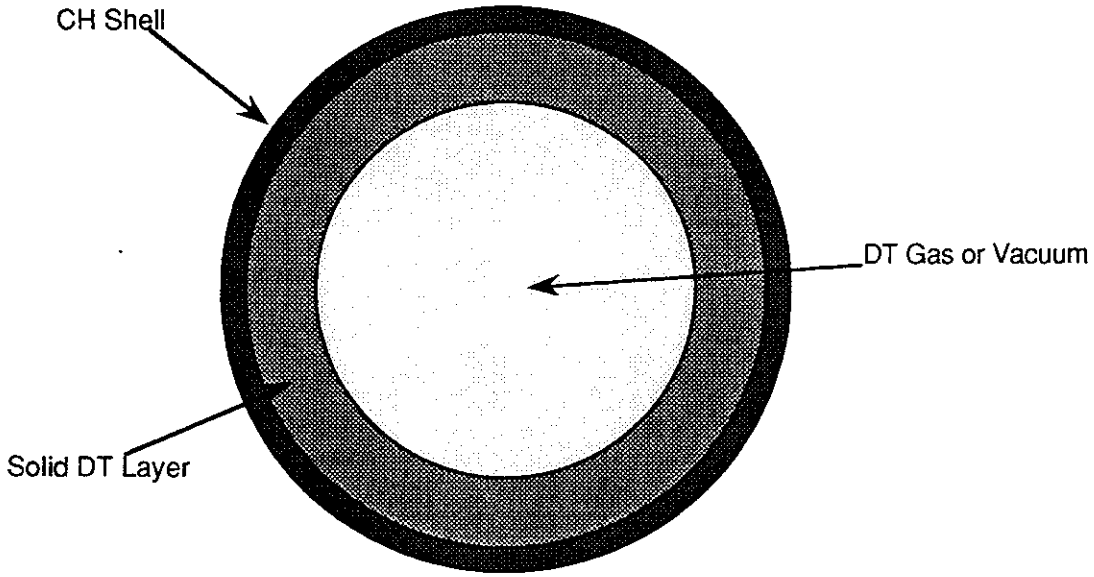

Figure 4.6.1-1 Schematic of Laser Direct-Drive IFE Target Structure.

In addition to the direct drive targets, the team also examined the indirect-drive laser IFE targets. It was assumed the fuel containing pellet or capsule of indirect-drive laser targets would be similar to the DD design. No further information on the geometry of laser indirect drive targets was supplied. As most of the information on these targets is classified, it is difficult to fill in the details needed to arrive at developing credible indirect-drive target illumination schemes. In considering the laser IFE indirect-drive (ID) target further, it was necessary to make a number of assumptions regarding ID laser targets based on the scant details available in the open literature. Additional details regarding these laser ID IFE target considerations can be found in Section 6.5.

A laser driver energy of 4 MJ was selected for reasons outlined in Sections 4.2 and 6.2. Mass scaling data was used to estimate that a target similar to that illustrated in Figure 4.6.1-1 scaled to a driver energy of 4 MJ would contain ~6.5 mg of DT and 16.5 mg of CH. This was used as the base target for the Prometheus-L design study. The possibility of adding thin layers of various materials to the basic DD target structure to act as permeation barriers, shine shields, etc., was also considered. However, with the possible exception of target alignment requirements, such additions were found to be unnecessary for the point design chosen. Therefore, the basic design shown in Figure 4.6.1-1 was used without modification.

Following the completion of the Prometheus-L laser driver design, a number of questions have emerged regarding the direct-drive target illumination requirements set forth by the TWG. Thus, when the requirements set forth by the TWG for direct-drive target illumination are compared with some of the known considerations applying to the laser beam illumination physics and the physics of light/plasma interaction, some serious questions arise regarding some of the TWG direct-drive target illumination requirements.[2] Facts and known requirements associated with the TWG guidelines, the laser driver, and target coupling physics are briefly summarized below.

4.6.1.1 Optimized Target Interactions - By considering the impacts of the TWG direct-drive target illumination requirements with the newly defined capabilities of the Prometheus-L laser driver and the known physics requirements of laser light/plasma interactions, it should be possible to optimize the laser/target coupling interaction significantly. This laser/target interaction optimization may result in a significant reduction in the laser energy required to reach a given DT target gain. The TWG has already specified that implementation of a "zoom" optical system which follows the imploding surface of critical density could guarantee an increase in target coupling efficiency of a factor of at least two.

Each of these three areas of discussion is briefly described below:

4.6.1.2 TWG's Direct-Drive Target Illumination Requirements - The TWG direct-drive target irradiation scenario includes the following elements:

(1) There will be at least 60 laser beams incident on the target.
(2) The target will be illuminated uniformly such that the intensity variation anywhere on the spherical surface will not vary more than ±1%.
(3) λ_{laser} ~ 250 nm, increasing the importance of Bremsstrahlung absorption over resonant absorption.
(4) The pulse duration of the main pulse will be approximately 6 ns with an approximately 60 ns lower intensity precursor "foot"; all beams must produce similar pulse shapes such that the uniformity requirement (2) is met.
(5) The laser beam size on the target will be equal to the target diameter.
(6) The spherical direct drive DT target will be approximately 0.6 cm in diameter.
(7) During the course of the laser pulse, the critical surface of the target will shrink to a diameter ~0.3 cm.
(8) The spatial intensity distribution of each laser beam incident on the target shall approximate $I(\theta) \sim (\sin \theta/\theta)^2$.

The penalty associated with failing to meet target illumination requirements is poor or no target yield.

4.6.1.3 Laser Driver Requirements/Characteristics - In addition to the preceding eight requirements set forth by the TWG, there are a number of requirements and/or characteristics of the laser driver and its associated optics which need to be taken into consideration.

(1) Excimer laser amplifiers produce optical beams having square cross-sections.
(2) Square laser beams map efficiently onto spherical surfaces only if the dimensions of the squares are significantly smaller than the sphere radius.
(3) The degree of trapezoidal apodization and the requirements for an efficient laser amplifier fill factor can be traded off to yield an optimum value.
(4) Optical elements cost least when sized according to an optimum aperture; optical vendors can be geared up to produce square (or rectangular) optics.
(5) Large aperture optics can be synthesized from an array of square (or rectangular) subelements using optimized aperture sizes.
(6) Trapezoidal (or pyramidal) laser beam apodization can reduce angular pointing requirements for the array mirrors.
(7) For a final focusing mirror focal length, f_m, of 40 m and an effective aperture, D_m, of 1 m, the f/number of the focusing optics is relatively large (~40).
(8) Automatic "zooming" of the optical system on the collapsing surface of critical density occurs when the foci of each of the 60 mirrors are located at the center

of the target. (This arrangement is impractical in the present case[2] since it would require a prohibitive number of beamlines.)

(9) For constant beam quality and laser wavelength, the far field focal spot size depends only on the f/number of the final focusing mirror; in the present case, the focal diameter for each laser beam is estimated to lie between 10 and 15 microns (assuming an f/40 system and λ = 248 nm).

(10) Research has been performed on high power optical techniques for generating negative non-linear refractive indices, thereby making possible (in principle) automatic "zooming" optical systems for high power lasers.

(11) The surface of the 0.6 cm diameter target sphere lies in the near field of each of the 60 laser beams, thereby permitting beams of predetermined shape and apodization to be placed on the target's critical surface (typically, laser beams do not follow spatial intensity profiles ~ $(\sin \theta/\theta)^2$ [this is a far-field diffraction intensity profile]).

(12) Although a variety of laser beam cross-sectional shapes and apodizations are possible, square beams with trapezoidal apodizations appear to be an optimum choice for efficiently placing a homogeneous intensity distribution on the spherical target surface.

(13) Even with careful computer control of the laser amplifier power conditioning, it will take strenuous efforts to achieve the ±1% target illumination homogeneity requirements set forth by the TWG.

The penalties for not heeding the physics of laser drivers are low efficiency, high driver cost, impaired performance, and difficult alignment problems.

4.6.1.4 Laser/Plasma Interaction Physics Requirements - The following observations regarding laser/plasma interactions can be made:

(1) The primary mechanism for coupling UV laser light into an imploding plasma having densities at or greater than the critical density is inverse Bremsstrahlung.

(2) Resonance absorption can also play a role, especially for large angles of incidence. In the case of linearly polarized laser light, resonance absorption is concentrated in two lobes aligned along the polarization vector.[3]

(3) Laser light interacts weakly with plasma below the critical density with the primarily effects being SBS, SRS, and refraction of the incident laser light.

(4) Laser light cannot propagate through plasmas having densities greater than critical density.

(5) Planar target interaction experiments have shown that the inverse Bremsstrahlung absorption depends upon the fifth power[3] of the cosine of the angle of incidence, q (where the angle of incidence is the angle between the

Poynting vector and the normal to the critical surface) for linear plasma density profiles and on the $(\cos\theta)^3$ for exponential plasma density profiles.

(6) Rayleigh-Taylor (RT) instabilities are driven primarily by laser beam intensity inhomogeneities occurring at the beginning of an implosion.

(7) Higher-order RT instabilities are more serious than low-order instabilities.

(8) Laser intensities above 10^{15} W/cm^2 tend to produce undesirable nonlinear optical effects in the plasma atmosphere (including stimulated Raman scattering, stimulated Brillouin scattering, harmonic generation at $\omega^{3/2}$, etc.).

(9) Resonance absorption (RA) depends upon the polarization vectors of each of the laser beams, which means that RA can spoil the homogeneity of target illumination even if the intensity is homogeneous. The TWG did not address the polarization issue.

The penalties associated with ignoring these plasma physics issues are inefficient light/plasma coupling, low target yield, and impaired system performance.

4.6.1.5 Global IFE Implications of Conflicting Requirements - The implications of this brief review of characteristics and requirements for the TWG direct-drive target prescription, the current laser driver design, and the physics of laser/plasma interactions are that significant improvements in IFE performance may be attained if careful tradeoffs are made to find optimum solutions which simultaneously satisfy all the requirements. This, then, is the purpose in examining these issues at this time so that unnecessary or inappropriate requirements which may actually impair IFE performance can be identified and, if possible, altered to permit a more optimum design to be generated.

4.6.1.6 Possible Conflicts Among the TWG Requirements: IB vs. RA - The two principal laser/plasma absorption mechanisms are inverse Bremsstrahlung (IB) and resonant absorption (RA). The TWG requirements that the direct-drive target be homogeneously (±1%) illuminated with ~60 randomly polarized laser beams equal to the diameter of the target may produce significant laser beam/plasma coupling inefficiencies and absorption non-uniformity. The most efficient excimer laser beam cross-section is rectangular, a shape which couples inefficiently onto a sphere unless the laser spot size is significantly smaller than the radius of the sphere. Furthermore, for full sphere illumination, most of the laser beam power will be incident on the critical surface of the target at incidence angles, θ_o, greater than 45° (when inverse Bremsstrahlung absorption[3] is proportional to $[\cos\theta_o]^5$) and additional laser/plasma coupling inhomogeneities due to resonant absorption may result. These problems are explored in detail below.

4.6.1.7 Calculation of Laser/Plasma Tangential Coupling Efficiencies for IB and RA - In general, calculations of laser/plasma coupling efficiency are extremely involved even when performed using magneto-hydrodynamics computer codes (i.e., LASNEX) on large machines. However, some simple considerations which can be performed on microcomputers are in order here. The first case considered is that of the specified target illumination scenario in which the incident laser beams are of dimensions equal to the diameter of the DT target. This scenario corresponds to the target illumination guideline furnished by the TWG. Both IB and RA calculations will be made. Resonant absorption (RA) depends approximately on $(\cos \theta_0)^2$, whereas for inverse Bremsstrahlung the absorption is proportional to $(\cos \theta_0)^5$ for linear plasma density gradients and proportional to $(\cos \theta_0)^3$ for exponential density gradients. The RA absorption also depends upon the polarization state of the absorbed laser light, and, in general, the RA absorption is a complex, two-lobed spatial function. Each of these two major light/plasma absorption mechanisms will be discussed below.

First, a specification is required for the laser pulse temporal format delivered in 60 beams to the direct-drive target in order to generate the target implosion scenario. An approximate sketch of each of the 60 laser beam pulses as specified by the TWG is shown below in Figure 4.6.1-2.

As indicated in Figure 4.6.1-2, the prepulse "ramp" precedes the main laser pulse in order to ablate a dilute plasma from the direct-drive DT target and form a critically-dense surface in preparation for arrival of the main pulse(s). At the end of the prepulse "ramp," the target is nominally still 0.6 cm in diameter, although the extent of the dilute plasma atmosphere ablated from the target is contained within a sphere of radius, R_a, given by the expression:

$$R_a = R_o + v_{plasma}\, \tau_{ramp} \qquad (4.6.1\text{-}1)$$

where $R_o \sim 0.3$ cm is the initial radius of the DT target, and where $v_{plasma} \sim 4 \times 10^7$ cm/sec according to measurements made by Auerbach[4], et al. For $\tau_{ramp} \sim 60$ ns, $R_a \sim 2.7$ cm. The primary linear effect of this spherical atmosphere of dilute plasma would be to refract the incident laser light slightly in such a manner that the converging beam would focus more quickly, but at a point well beyond the target. The tangential target illumination geometry which occurs at the beginning of the main laser pulse is shown in Figure 4.6.1-3.

It is presumed that the dilute plasma atmosphere surrounding the target only produces a slight focusing of the incident rays. As discussed below, however, the nonlinear effects (stimulated Brillouin scattering, stimulated Raman scattering) can produce a significant number of hot electrons which can lead to target preheat.

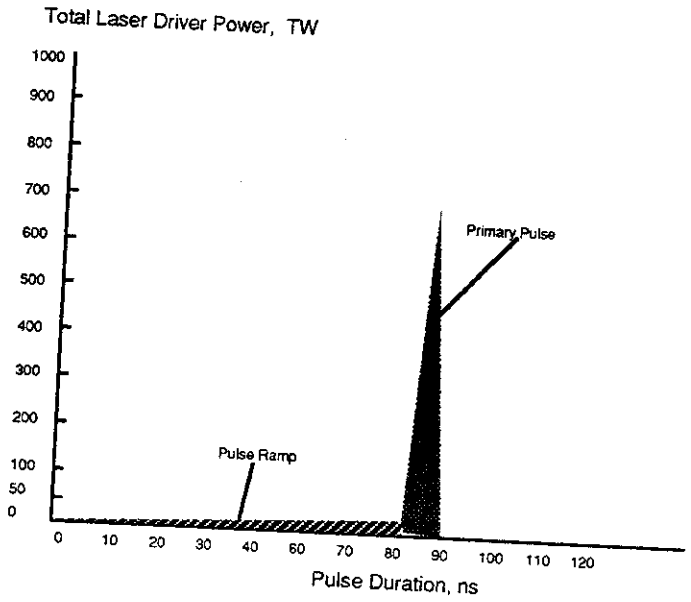

Figure 4.6.1-2 The Laser Pulse Features a 80 ns Prepulse Containing 30% of the Energy

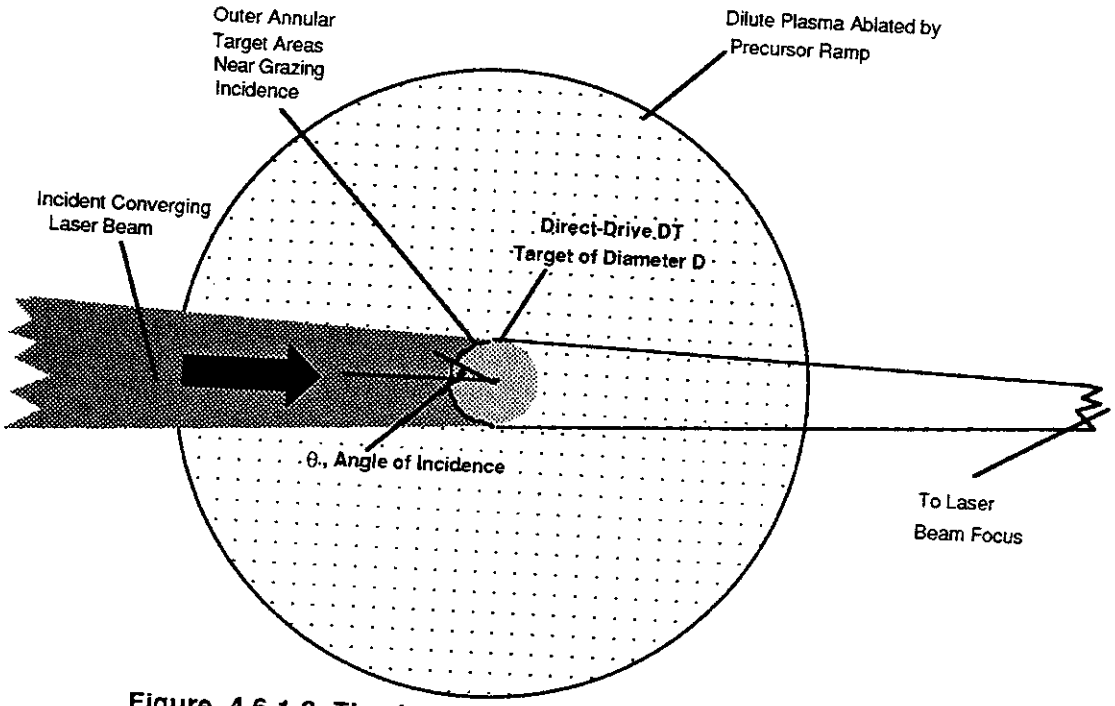

Figure 4.6.1-3 The Laser Prepulse Ablates a Dilute Plasma Atmosphere 3.2 cm Deep from the Target

Inverse Bremsstrahlung Absorption - It is apparent from Figure 4.6.1-3 that most of the incident laser power will be incident on the target critical surface at angles greater than 45°. Numerous well-characterized, laser-induced plasma experiments have been conducted on planar targets for which the angle of incidence, θ_o, was well known. An expression[3] for the fractional absorption, f_{ib}, as a function of θ_o due to inverse Bremsstrahlung for a plasma is:

$$f_{ib} = \left(\frac{16\nu}{15\omega}\right) \kappa\Delta R \cos^5\theta_o \qquad (4.6.1\text{-}2)$$

where the ratio ν/ω is evaluated at the critical density. Since the focal ratio of the laser driver is ~f/40 to first order, the incident laser beams can be regarded as plane waves. Simple laser/plasma absorption calculations have been carried out using Eq. 4.6.1-2 for λ = 248 nm, assuming a "top-hat" beam intensity profile apodization and that the $f_{ib}(\theta_o = 0) \sim 1$ on the surface of critical density. The results are shown below in Figure 4.6.1-4 for a time immediately prior to the target implosion.

Although these calculations were carried out using a larger laser amplifier fill factor than the $(\sin\theta)^2/\theta^2$ apodization assumed by the TWG, efficient extraction from excimer laser amplifiers (and the Raman accumulators) would involve the use of high efficiency apodizations and not be limited by far field diffraction profiles such as $(\sin x)^2/x^2$. Using the top-hat apodization and assuming that the laser beam spot sizes are equal to 0.6 cm, then the laser energy is absorbed by the target as a function of the target diameter and angle of incidence. This relationship is shown in Figure 4.6.1-5.

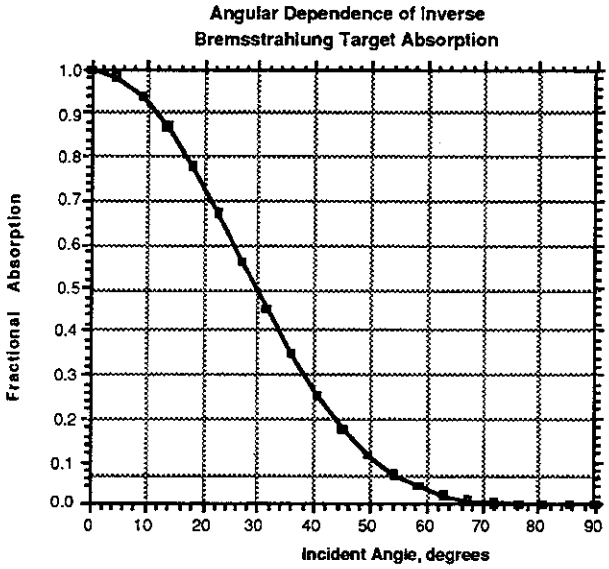

Figure 4.6.1-4. The Laser/Plasma Inverse Bremsstrahlung Absorption Fraction Depends on the Incident Angle, θ_o

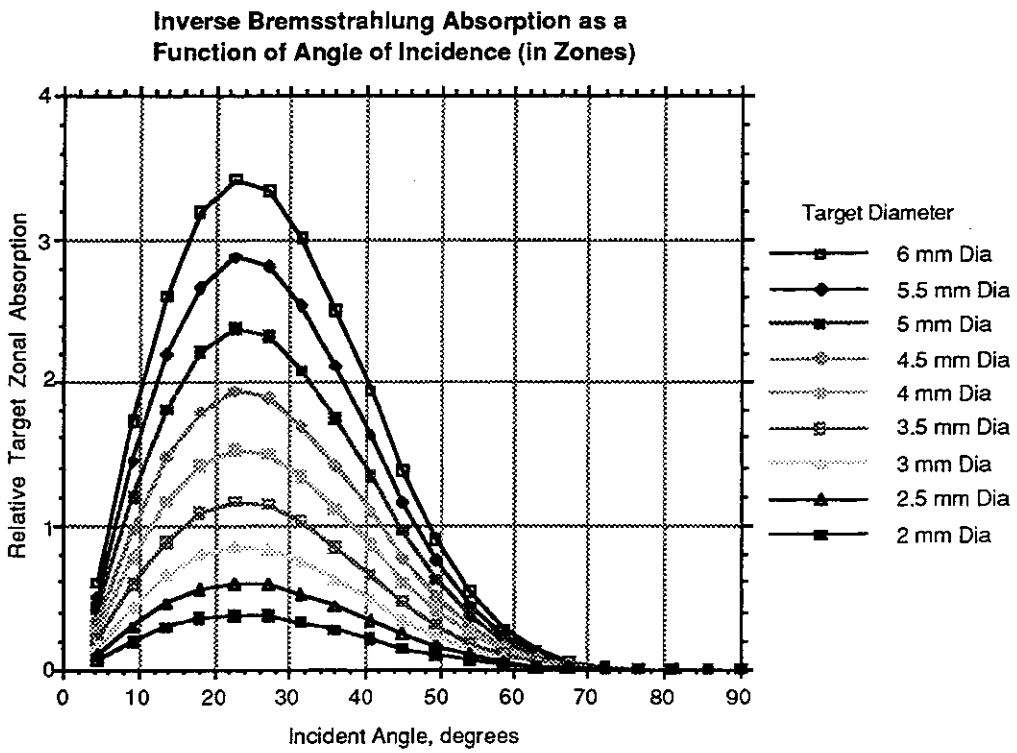

Figure 4.6.1-5. The Inverse Bremsstrahlung Energy Absorbed by Direct-Drive Targets Depend on the Incident Angle and Target Diameter (6 mm diameter spot size, 100 kJ beam, 6 ns pulse duration, top-hat apodization)

The initial amounts of absorbed laser energy are small in Figure 4.6.1-5 since the areas of the annular apertures are reduced for small values of θ_o. The geometry used for conducting these calculations is shown below in Figure 4.6.1-6.

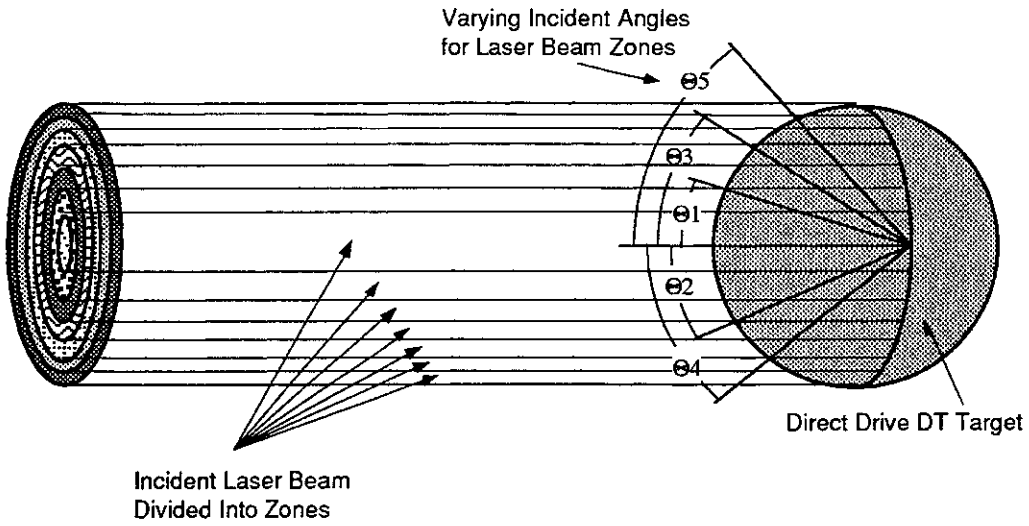

Figure 4.6.1-6 The Incident Laser Beam Can Be Decomposed Into Annular Zones to Calculate Absorption Efficiencies

The variation of the absorbed laser energy/beam for inverse *Bremsstrahlung* as a function of target diameter was calculated assuming that the diameter of the critical surface remains constant during the entire high power pulse duration (which was assumed to be a temporal top hat distribution as well) and the results are shown below in Figure 4.6.1-7.

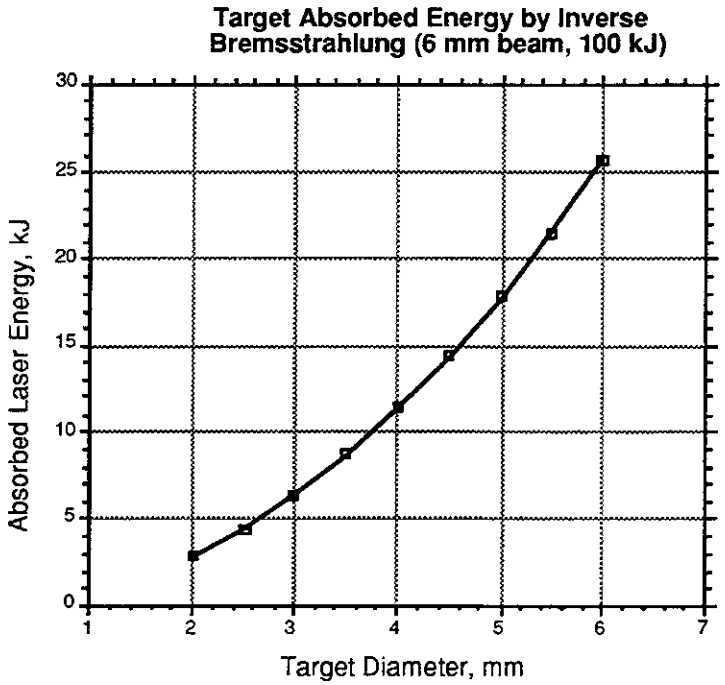

Figure 4.6.1-7 The Absorbed Laser Energy/Beam Depends on the Direct Drive Target Diameter for Inverse Bremsstrahlung (assuming 100 kJ/Beam and 6 mm diameter laser spot sizes) for Static Target Diameters

As indicated, when the critical density target diameter decreases to a value of R_T ~ 3 mm, the laser power couples only approximately 7% into the target. Although it was assumed that the radius of the target remained constant during the laser pulse in calculating the results for Figure 4.6.1-7, it is straightforward to estimate the energy absorbed by the target as it implodes. Thus if the rate of target implosion, dR_T/dt, is constant (here $dR_T/dt \sim 2.5 \times 10^7$ cm/sec) during the main portion of the laser pulse, then the total energy absorbed by the target is calculated from the expression:

$$E_{tot} = \frac{1}{N} \sum_{k=0}^{N} E_{abs}(R_k) \qquad (4.6.1\text{-}3)$$

where N is the number of iterations taken between $R_1 = 3$ mm and $R_N = 1.5$ mm. Taking the further approximation that the laser power is constant during the implosion of the target, then the energy absorbed by the target is calculated from Eq. 4.6.1-3 to be 15.2 kJ/beam line, or approximately 15% of the available laser energy. Much of the

laser light simply misses the critical surface of the target under these circumstances. This geometry is illustrated below in Figure 4.6.1-8.

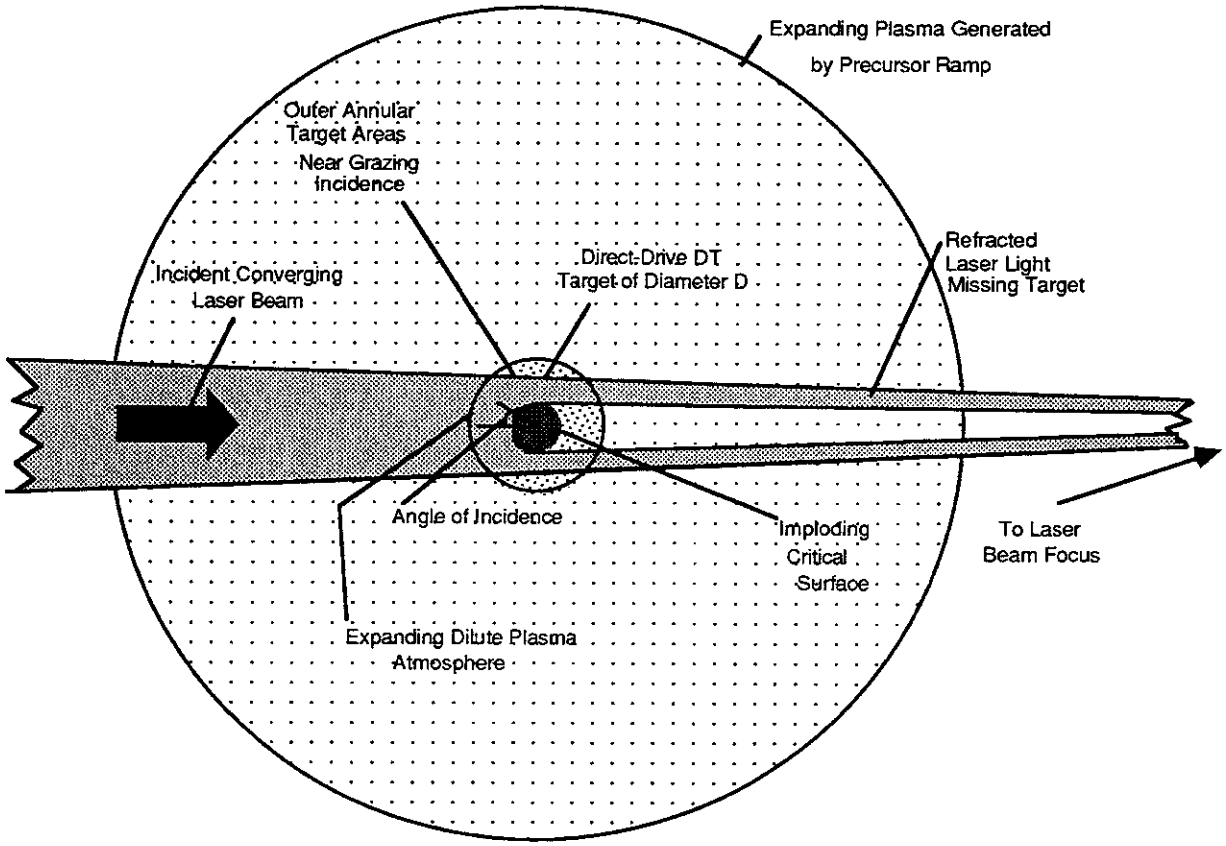

Figure 4.6.1-8. The Direct Drive Target Diameter Implodes to Half the Laser Beam Diameter by the End of the Main Laser Pulse

Resonance Absorption Calculations - The energy absorbed by resonant-driven fields in the plasma is described by the expression:[3]

$$E_{abs} = \int \frac{\upsilon(<E_r^* E_r>)}{8\pi} r^2 \, dr \, \sin\theta \, d\theta \, d\phi \qquad (4.6.1\text{-}4)$$

where E_r is the radial electric field of the laser beam. Near the critical density, the expression for E_r is given by:

$$E_r = \frac{\ell(\ell+1)}{(i\varepsilon k^2 r^2)} a_1 \left(\ell - \alpha_\ell^2\right)^{\frac{1}{4}} P_\ell^1(\cos\theta) \cos\phi \exp(i\delta) \frac{\Phi^2(\tau_1)}{2\pi\gamma\alpha_\ell^2} \qquad (4.6.1\text{-}5)$$

where a_l is given by the expression:

$$\alpha_\ell = \frac{\sqrt{\ell\,(\ell+1)}}{k\,R_c} \qquad (4.6.1\text{-}6)$$

(where R_c is the radius of the plasma critical density) and where $\Phi^2(\tau_l)$ is the absorption function for the lth mode. The fraction absorption of the lth mode, f_{RA}, is given by:

$$f_{RA} = \frac{\Phi^2(\tau_l)}{2\pi} \sqrt{1 - \alpha_l^2} \qquad (4.6.1\text{-}7)$$

so that the total power absorbed from the laser beam as a consequence of resonance absorption is given by:

$$P_{RA} = \sum_l \frac{P_l}{2\pi} \Phi^2(\tau_l) \sqrt{1 - \alpha_l^2} \qquad (4.6.1\text{-}8)$$

where P_l is the laser power in the lth mode.

The net result of performing the integral in Eq. 4.6.1-4 is to show that resonance absorption generally depends upon $(\cos \theta_o)^2$. Perhaps a more serious result of these analyses[3] is that the spatial absorption distribution function is not uniform over the target sphere. The calculated RA distribution for a vertically polarized laser beam is shown in Figure 4.6.1-9.

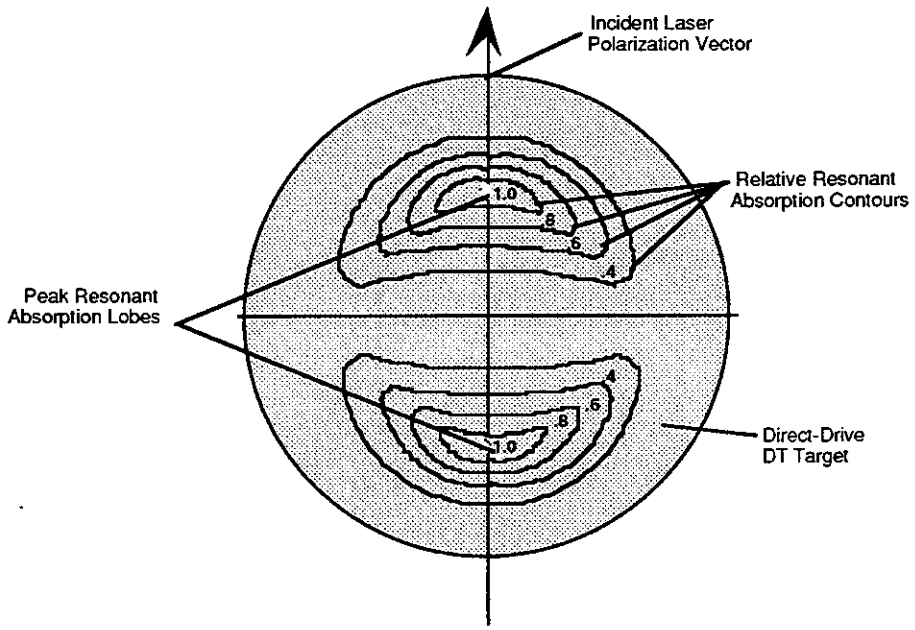

Figure 4.6.1-9. The Calculated Spatial Dependence of the Laser Power Absorbed by Resonance Absorption Is Not Homogeneous

As shown, resonance absorption is predicted to produce two symmetrical "hot spots" of absorption at mid-latitudes on the sphere when illuminated with linearly polarized light. This may constitute an absorption uniformity problem because this process occurs even when the sphere is uniformly illuminated. However, by using λ = 248 nm

laser radiation, the effects of resonance absorption are not expected to be reduced relative to inverse Bremsstrahlung.

Simple laser/plasma absorption calculations have been carried out using Eq. 4.6.1-7 and Eq. 4.6.1-8 for $\lambda = 248$ nm, assuming a "top-hat" beam intensity profile apodization and assuming that $f_{ra}(\theta_o = 0) \sim 1$ (and $f_{ra} = \xi\,[\cos\theta]^2$) on the surface of critical density. The results are shown below in Figure 4.6.1-10 for the case prior to the implosion.

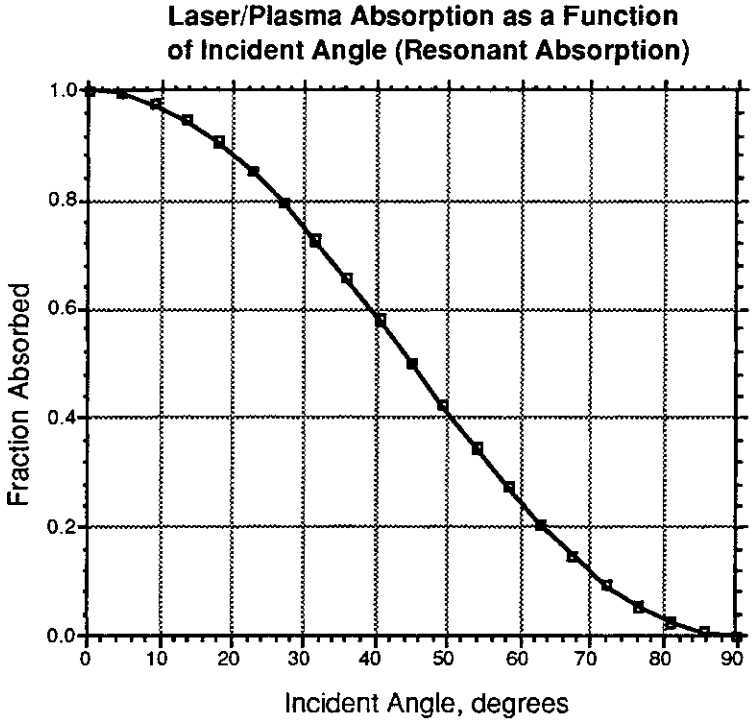

Figure 4.6.1-10. The Fraction of Laser Power Absorbed Via Laser/Plasma Resonance Absorption Is a Function of the Incident Angle, θ_o

As before, although these calculations were carried out using a "top-hat" intensity profile (i.e., a larger laser amplifier fill factor than the $(\sin x)^2/x^2$ apodization assumed by the TWG), efficient extraction from excimer laser amplifiers (and the Raman accumulators) would involve the use of such high efficiency apodizations. Using the top-hat apodization and assuming that the laser beam spot sizes are equal to 0.6 cm, then the laser energy absorbed by the target as a function of target diameter and angle of incidence is shown in Figure 4.6.1-11.

As calculated above for the inverse Bremsstrahlung case, the initial amounts of absorbed laser energy are small in Figure 4.6.1-11 since the areas of the annular apertures are reduced for small values of θ_o, in accordance with the calculation procedure illustrated in Figure 4.6.1-6.

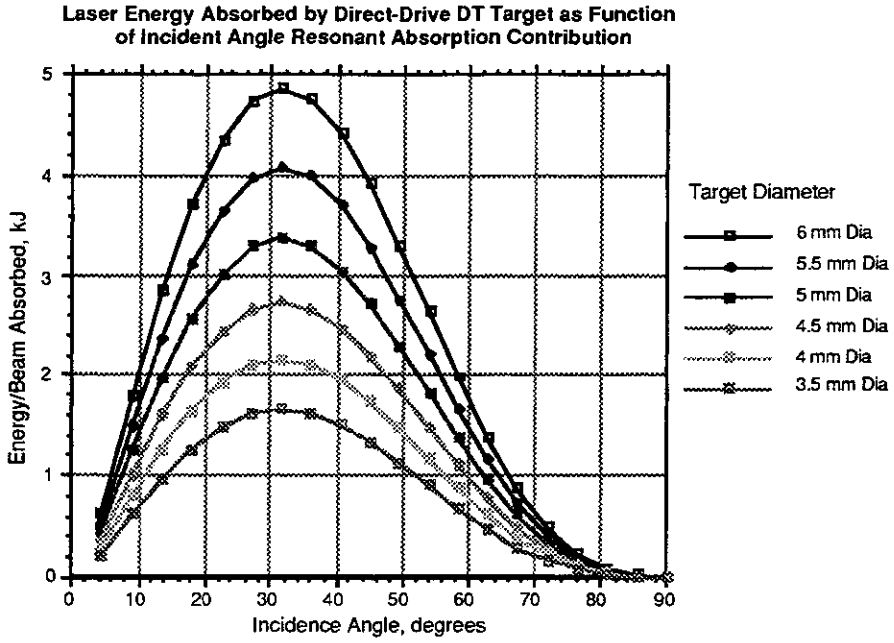

Figure 4.6.1-11. The Resonance Absorbed Energy for Direct-Drive Targets is a Function of Both Incident Angle and Target Diameter (6 mm diameter Spot Size, 100 kJ Beam, 6 ns Pulse Duration, Top-Hat Apodization)

Following in a manner similar to that for the IB case above, the variation of the absorbed laser energy/beam for inverse Bremsstrahlung as a function of target diameter was calculated assuming that the critical surface remains constant at a constant diameter during the delivery of the high power laser pulse (which was assumed to be a temporal top hat distribution as well) and the results are shown in Figure 4.6.1-12.

As indicated in Figure 4.6.1-12, when the critical density target diameter is reduced to $R_T \sim 3$ mm (with the laser beam diameter equal to 6 mm), the laser power couples only approximately 11% into the target. The target radius was held constant during the arrival of the laser pulse in calculating the results for Figure 4.6.1-7. It is straightforward to estimate the energy absorbed by the target as it implodes using Eq. 4.6.1-1 above; it is calculated that 27.7 kJ/beam would be absorbed by the target (assuming resonant absorption accounted for 100% of the laser/plasma target interaction) or approximately 28%, based on the approximations that $f_{RA}(\theta_o = 0) = 1$, and $f_{RA}(\theta_o) = \xi(\cos \theta_o)^2$.

In actual fact, resonance absorption is not the primarily laser/plasma absorption mechanism and, consequently, the fraction of laser light, ξ_{RA}, absorbed by the resonance absorption mechanism must be added to the fraction of laser light absorbed by inverse Bremsstrahlung, ξ_{RA}, to produce a total absorption, ξ_{tot}, given by

$$\xi_{tot} = \xi_{IB} + \xi_{RA} \qquad (4.6.1\text{-}9)$$

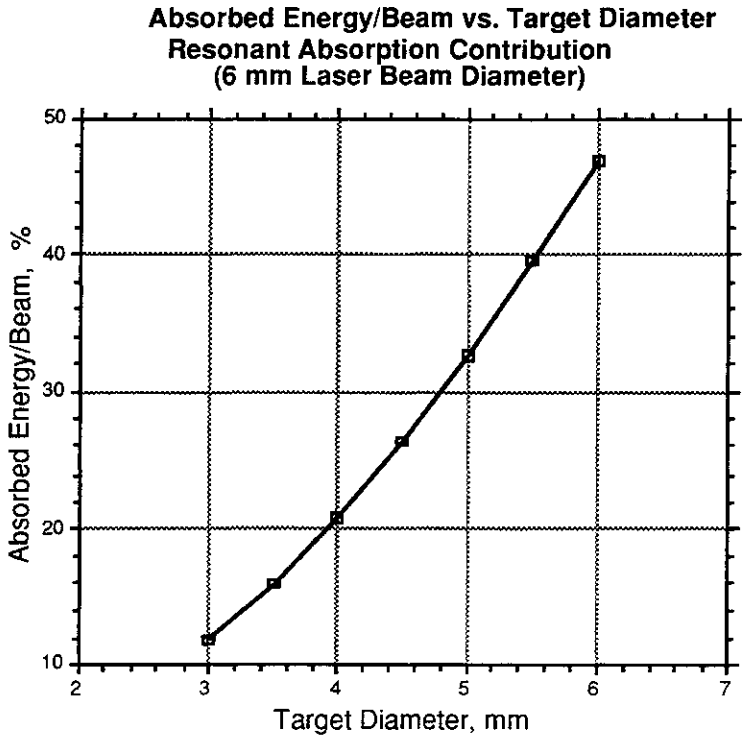

Figure 4.6.1-12. Estimated Absorbed Laser Energy/Beam vs. Direct Drive Target Diameter for Resonance Absorption (100 kJ/Beam, 6 mm Diameter Laser Beam) Assuming Constant Target Diameter

Comparison of the Target Absorption Results of IB and RA - As indicated above, simple incident angle-dependent calculations regarding resonant absorption have produced the results that only approximately 28% of incident laser light would be absorbed by a 6-mm diameter sphere that uniformly implodes to a diameter of 3 mm during the laser pulse. The previous result calculated for inverse Bremsstrahlung under the same circumstances produced a value of ξ_{IB} ~ 15%. If it is assumed that IB accounts for approximately two-thirds of the target absorption and RA the remaining one third, then the overall absorption efficiency of a tangentially-illuminated 6 mm DT direct-drive target would be approximately 20%. Thus, for a laser energy of 5 MJ delivered to the target, these rough estimates suggest that only 1 MJ would be coupled into the target!

4.6.1.8 Calculation of Laser/Plasma Nested Trapezoidal Beam Coupling Efficiency - In a similar manner, the coupling efficiency for a laser beam with a trapezoidal apodization focused down to an intermediate spot size, δ_{laser}, given approximately by the expression:

$$\delta = R_T \sqrt{\frac{4\pi}{N}} \qquad (4.6.1\text{-}10)$$

where, as before, R_T is the radius of the direct-drive DT target and N is the number of laser beams (N ~ 60). In the case in which R_T ~ 0.6 cm, then δ_{laser} = 0.137 cm and θ_{max} ~ 26.2°.

A schematic of meshing trapezoidal intensity distributions is illustrated in Figure 4.6.1-13.

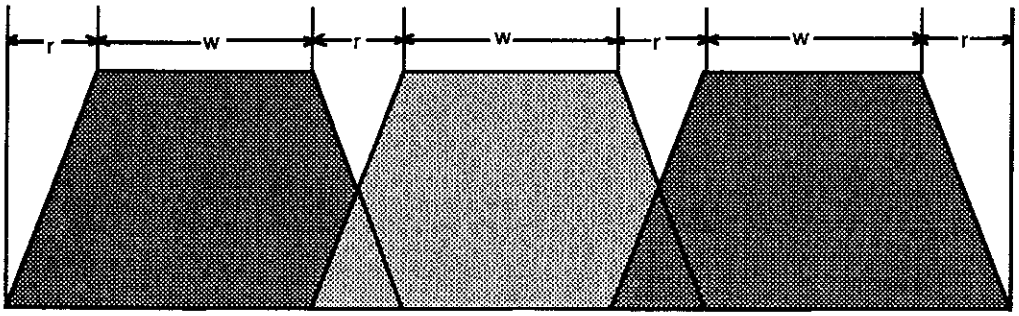

Figure 4.6.1-13. Meshing Trapezoidal Intensity Distributions Permits Smooth Near-Field Illumination of Direct Drive Targets

By varying the fill factor of these trapezoidal beams, the relative interbeam alignment accuracy of the optical system can be traded off against laser amplifier efficiency (i.e., steep trapezoidal shoulders [large w/r ratios] mean high amplifier efficiency). Figure 4.6.1-13 illustrates a case of a high w/r ratio. An example of nested trapezoidal beams with a low w/r ratio is shown below in Figure 4.6.1-14. Since these beams are in the near field (with a Fresnel number > 100), relatively detailed apodization profiles are possible, although the impact of the apodization on the amplifier apodization must be calculated.

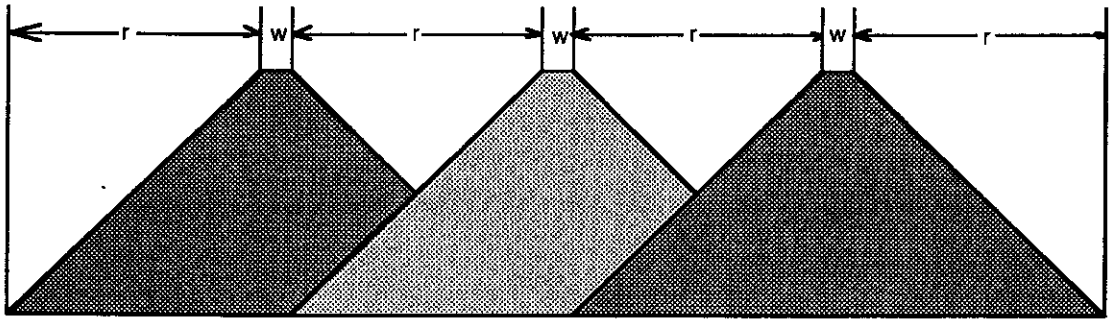

Figure 4.6.1-14. Meshing Trapezoidal Intensity Distributions with Low w/r Ratios Relaxes Near-Field Laser Beam Alignment Tolerances

In practice, it may be important to include the capabilities of on-board computer control systems to permit interferometric alignment accuracy of the final focusing mirrors onto a surrogate target to be attained. Precise erection of a surrogate target at the center of the target chamber would be a key feature of permitting laser beams to be aligned to

submicroradian accuracy. Such precise angular alignment must be carried out for both q and f corresponding to the two beveled directions of the trapezoidal apodization. An isometric view of the trapezoidal apodization is shown below in Figure 4.6.1-15.

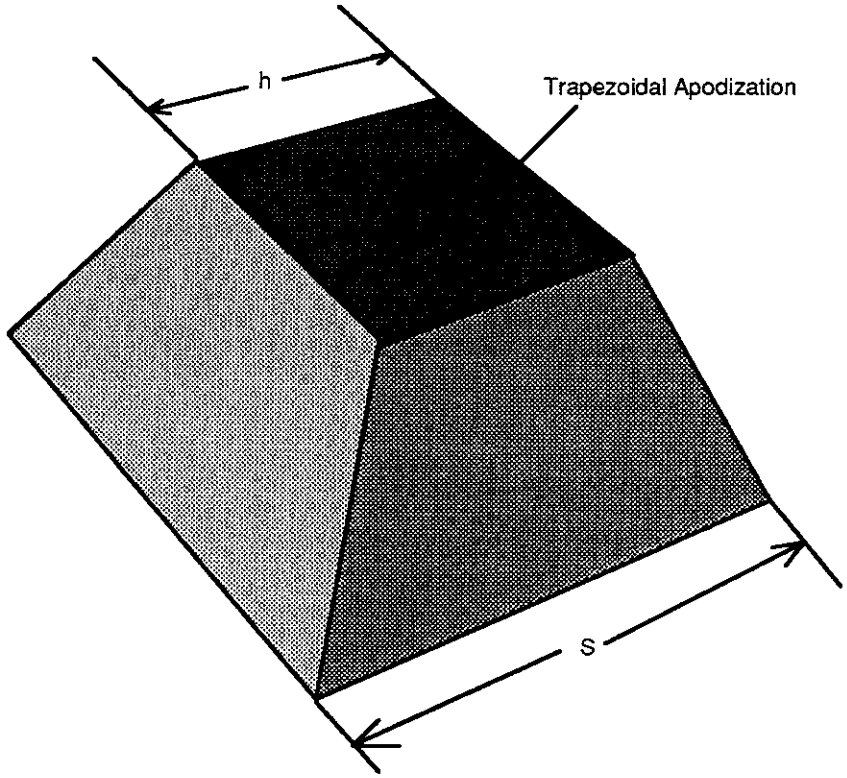

Figure 4.6.1-15. An Isometric View of Trapezoidal Beam Illustrates the Interlocking of Multiple Near-Field Laser Beams Aligned on Direct Drive Fusion Targets

The use of nested trapezoidal beams can be applied to direct-drive targets illuminated with a variety of beam architectures. Considered briefly here are beam configurations starting with cubic symmetry (for which N = 6) and going out as far as N = 240. The nested trapezoidal parameters for these cases are summarized in Table 4.6.1-1.

Table 4.6.1-1
Parameters for Direct-Drive Nested Trapezoidal Beam Arrangements

No.	No. of Beams	Spot Size on Target (mm)	Coupling Efficiency (%)
1	6	4.34	47.4
2	12	3.07	69.2
3	20	2.38	80.4
4	28	2.01	85.6
5	32	1.88	87.3
6	60	1.37	93.1
7	80	1.19	94.8
8	120	0.97	96.5
9	240	0.69	98.2

The laser/target coupling efficiencies tabulated in Table 4.6.1-1 were calculated using Eq. 4.6.1-2 above with the incident laser beam decomposed into annular zones as shown in Figure 4.6.1-6 above, assuming that the diameter of the critical surface was remaining constant.

The near field focusing geometry of the trapezoidal nesting of laser beams is illustrated for a single incident laser beam in Figure 4.6.1-16.

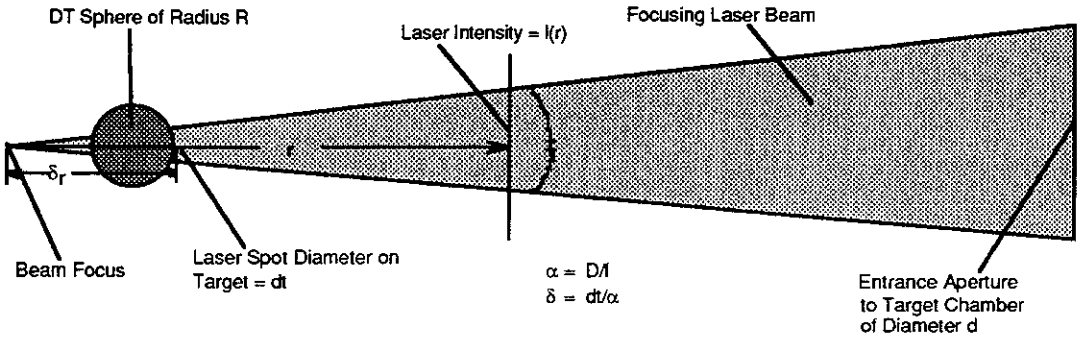

Figure 4.6.1-16. Near-Field Focusing Geometry for Trapezoidal Nesting

Since the DD target is located in the near field, the positional accuracy, $d = \Delta x$, of each beam incident on the target sphere is related to the required DD target illumination uniformity, Ψ, and the trapezoidal spacing parameter, r, via the simple relation:

$$d = \Delta x = \Psi r \qquad (4.6.1\text{-}11)$$

Thus, if the TWG requirement for the required DD illumination uniformity (Ψ) is equal to 0.01, then $\Delta x = r/100$. The angular pointing requirement, $\Delta\theta$, of the GIMM would therefore be given by the expression:

$$\Delta\theta = d/(R1) = \Psi r/R1 \qquad (4.6.1\text{-}12)$$

where R1 is the distance from the GIMM to the target. The values for the summit width of the trapezoid, w (see Figure 4.6.1-13 and 4.6.1-14 for a definition of w), are calculated as a function of the number of laser beam lines, N, and the results presented above in Table 4.6.1-1. For a fixed target diameter (d = 0.6 cm), there are other limitations on r since, in addition to optical alignment accuracy, $\Delta\theta$, r affects the laser beam fill factor, ξff. An expression for ξff is given by:

$$\xi_{ff} = \frac{w^2}{w^2 + 2r(w + r)} \qquad (4.6.1\text{-}13)$$

where w and r are defined previously. In order for laser amplifier power extraction to be efficient and to minimize optical damage, it is important that ξff ~ 1, which would force r = 0. This would be undesirable for the requirement noted above for the

alignment accuracy, $\Delta\theta$. As shown below in Figure 4.6.1-17, a ray from an alignment laser would be deflected in angle, $\Delta\alpha = 2d/R$, assuming that a shine shield is available on the DD target to assist in target alignment.

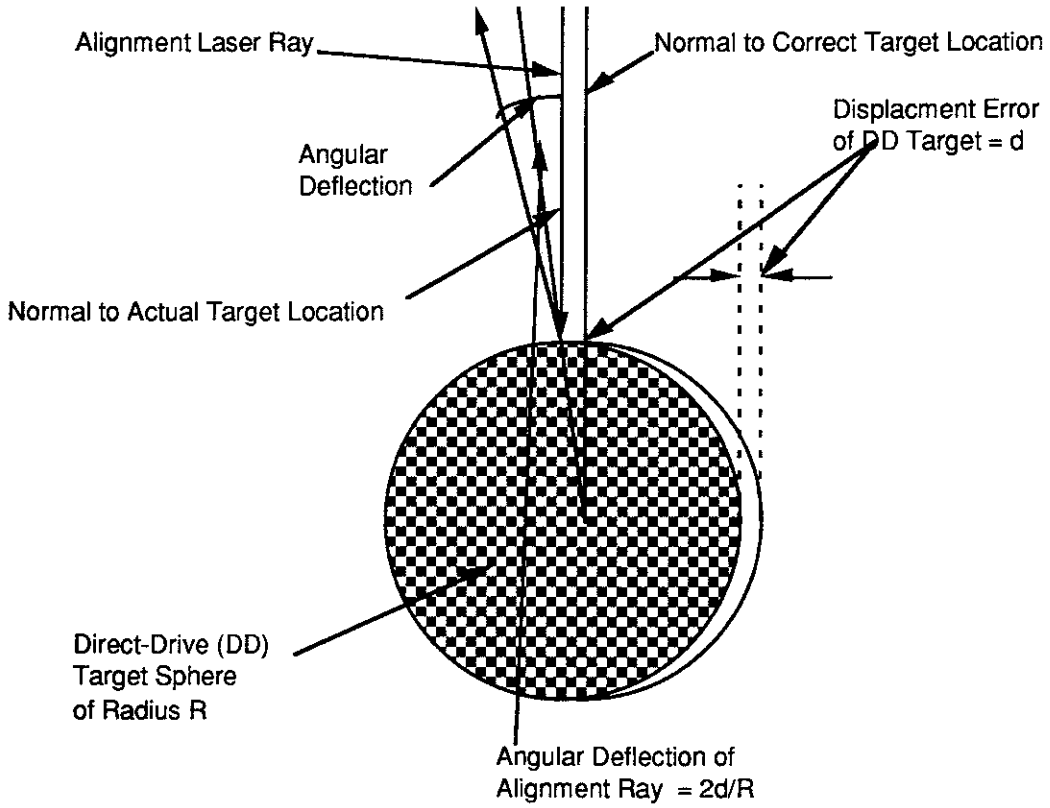

Figure 4.6.1-17 DD Target Misalignment Geometry for Alignment Laser Reflecting Off of Shine Shield: Angular Deflection = $\Delta\alpha$.

The dependence of the laser beam fill factor, ξff, on r is illustrated in Figure 4.6.1-18 for the cases of N = 60, 80, and 120 beams.

If values of the Prometheus-L laser beam fill factors, ξff > 0.8, are desired, then for 60 beams, w = 0.137 cm, r = 0.017 cm, and the alignment accuracy, $\Delta\theta$, equals $\Psi r/R1 \sim 9\times10^{-8}$ radians or ~0.1 μR. The corresponding sensing angle, $\Delta\alpha$, from the DD target shine shield is ~2r/R ~ 100 μR. Although these are challenging requirements for the Prometheus-L laser/target beam alignment system, the resulting cost reductions possible may be worth the additional technical investment.

The laser/target coupling efficiency, ξ, is plotted as a function of the number of laser beams in Figure 4.6.1-19. To be conservative, these calculations included only the $f_{IB} = \xi(\cos\theta_o)^5$ inverse Bremsstrahlung contributions and did not include any resonant absorption components.

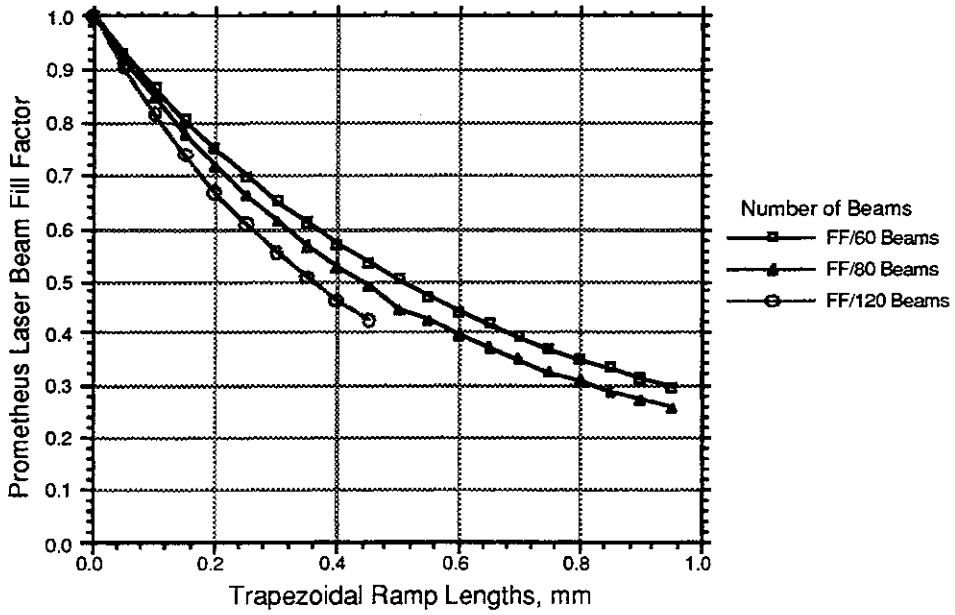

Figure 4.6.1-18 Laser Beam Fill Factors as a Function of Trapezoidal Ramp Lengths, r.

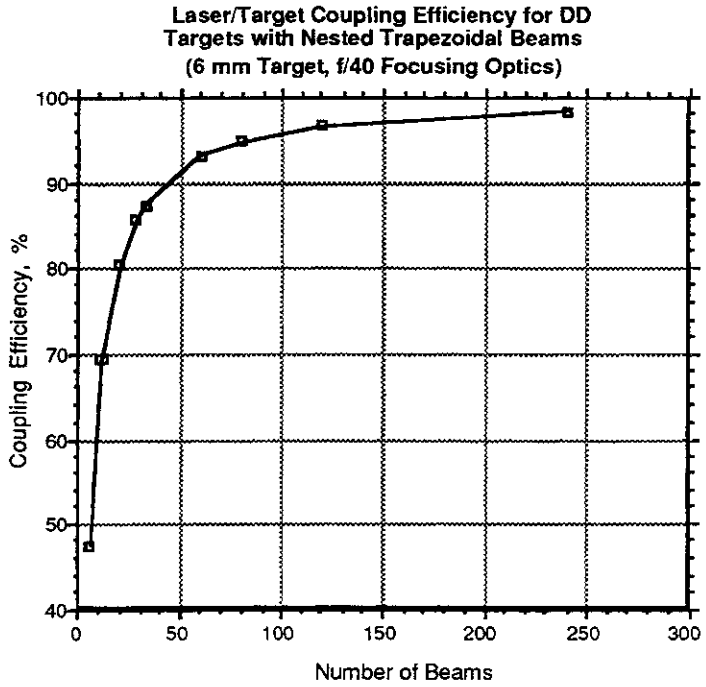

Figure 4.6.1-19. The Laser/Target Coupling Efficiency, ξ_T, Depends on the Number of Laser Beams Illuminating the Direct Drive Target (Constant 6 mm DD DT Target Diameter and IB Interaction)

As shown for large numbers of laser beams, the laser/plasma coupling efficiency exceeds 90% for a static target. When these calculations are repeated for N = 60 for critical surfaces ranging from 6 mm to 3 mm diameters while keeping the beam diameter at the target constant (~1.37 mm), the coupling efficiency, ξ_T, drops from 93% to 75%, as illustrated in Figure 4.6.1-20.

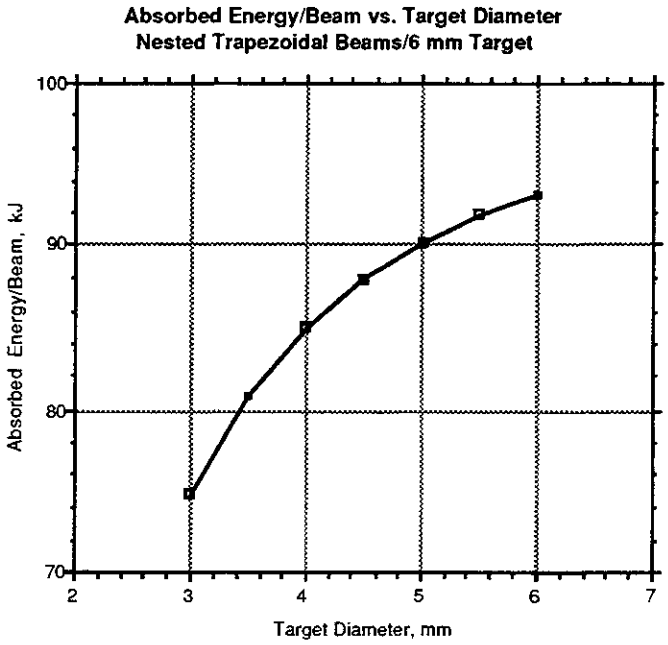

Figure 4.6.1-20. The Laser/Target Coupling Efficiency, ξ_T, Depends on the Critical Surface Target Diameter (60 Beams, f/40 Optics, 1.37 mm Spot Size, Trapezoidal Beam Nesting)

When the variation of laser target coupling efficiency with imploding target diameter is calculated, the integrated energy absorbed by the imploding target was calculated to be 86.2% of the incident laser energy for the 60 beam case, 6 mm DT target, f/40 optics, and trapezoidal beam nesting. This is to be compared with the 20% integrated coupling efficiency calculated for the tangential target illumination case above.

4.6.1.9 Summary of Laser/Target Interaction Physics - During the course of designing the IFE KrF laser driver, some questions have arisen with regard to the final focusing requirements in order to achieve efficient target coupling. The TWG guideline has adopted a conservative approach by illuminating the target with at least 60 beams having diameters at the target approximately equal to the diameter of the target. Elementary calculations of the laser/plasma coupling assuming that the primary coupling process is inverse Bremsstrahlung suggest that this conservative approach may result in less than 15% of the laser beam energy actually being coupled into the target (with an estimated additional 5% absorption coming from resonant absorption for a total of 20%). Similar IB calculations carried out for trapezoidal beam nesting to

minimize the angle of incidence with the critical surface while maintaining illumination homogeneity suggest that approximately 85% of the laser beam energy can be coupled into the target. These calculations also suggest that the importance of "zooming" the laser beams to follow the imploding critical surface is not as important for trapezoidal beam nesting as for tangential target illumination. Thus, there is evidence that we should be able to take advantage of the "zoomed optics" benefit in calculating the amount of laser energy necessary to drive a given target. A potential key problem with the trapezoidal beam nesting is intensity inhomogeneities arising from beam overlapping on the imploding target. This is illustrated in Figure 4.6.1-21.

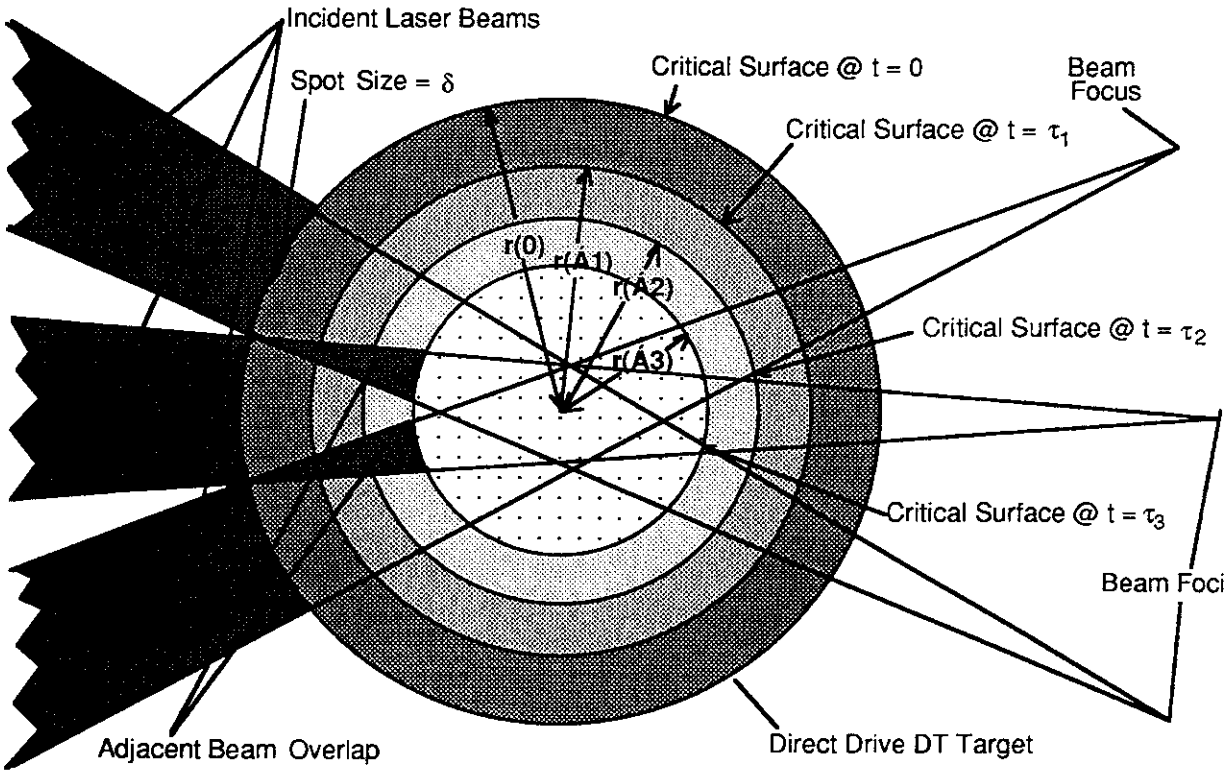

Figure 4.6.1-21. The Imploding Direct Drive Target Critical Surfaces Requires Zooming of the Near-Field Laser Beams to Maintain Homogeneous Illumination

Since this overlapping would occur late in the target implosion, it is thought likely that no Rayleigh-Taylor instabilities would be driven by this overlap.

Lastly, these considerations raise a concern that even if we were to achieve the remarkable level of illumination homogeneity (±1%) defined in the TWG Guidelines, the two-lobe absorption distribution of resonant absorption (Figure 4.6.1-9) may make this stringent illumination homogeneity specification meaningless.

4.6.2 Heavy Ion Driver Targets - In direct analogy with the two types of laser-driven (LD) IFE targets, there are two general types of Heavy Ion Driver (HID) targets: (1) direct drive targets, and (2) indirect drive targets.

Although these HID targets bear some general similarities with their laser-driven target counterparts, there are some significant structural differences in the HI targets as well as major differences in the energy coupling mechanisms to the targets. For example, the HI driver delivers a 6 ns pulse containing approximately 6 MJ of energy in the form of non-relativistic, high-Z ions having an energy per ion of approximately 4 GeV. This 6 MJ of energy is assumed to be stopped in a relatively thin layer of converter material. The LD, on the other hand, delivers a 6 ns laser pulse containing approximately 4 MJ of energy in the form of ultraviolet photons having wavelengths of approximately 250 nm.

4.6.2.1 Heavy Ion Direct Drive Target Description - At first glance, the design of the Heavy Ion Driver (HID) direct-drive target is similar to the LD direct-drive target illustrated in Figure 4.6.1-1. A diagram of the HID direct-drive target is presented below in Figure 4.6.2-1.

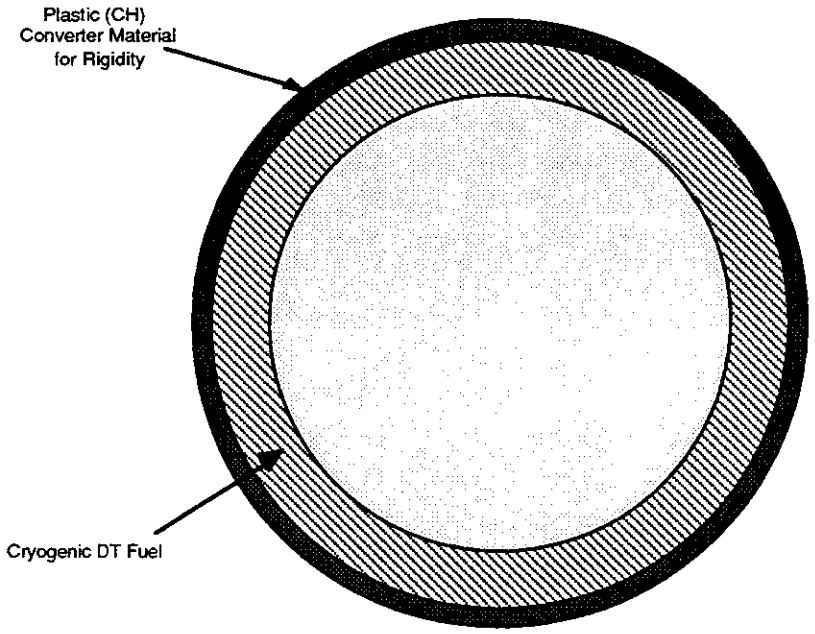

Figure 4.6.2-1 The Direct Drive HID Target Has Spherical Symmetry and Requires Uniform Power Loading of its Converter Shell

As indicated, the HID direct-drive target is a spherical, multi-shelled structure containing successive layers of converter material, structural CH (as needed for robust target construction), and cryogenic DT located at the center of the target. An alternative design is shown in Figure 4.6.2-2.

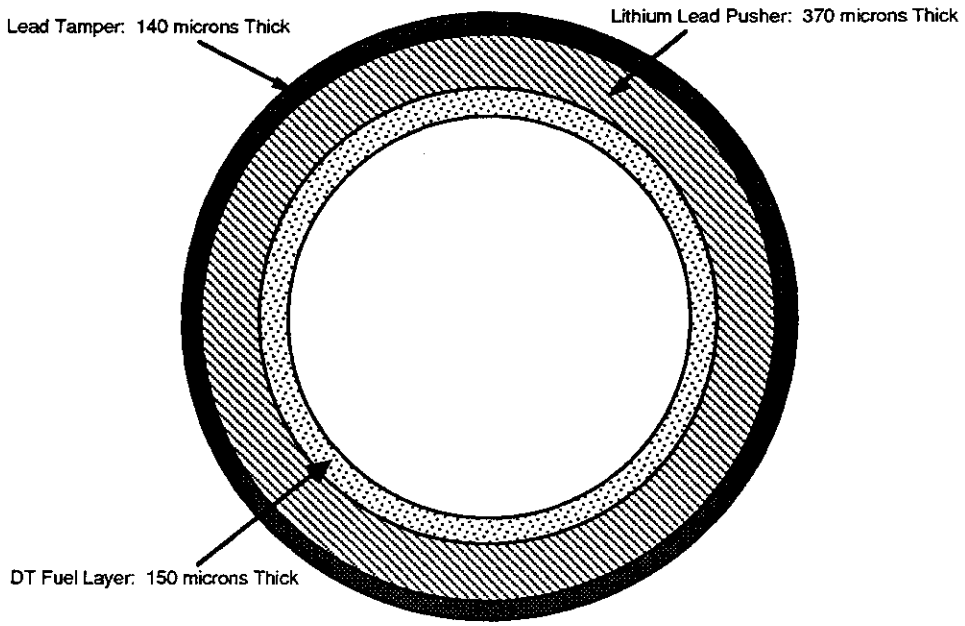

Figure 4.6.2-2. Alternative Direct Drive HID Target with Pb Tamper and Li-Pb Pusher (HIBALL-I)[5]

Heavy Ion Driver (HID) direct-drive targets yield fusion energy based upon the following scenario. At a time t = 0, the spherical HID direct-drive target is enveloped by approximately 100 HID beams symmetrically focused on the converter shell of the HID direct-drive target and synchronized to achieve the required degree of power loading uniformity. These focused HID beams consist of non-relativistic ions having individual energies of approximately 4 GeV. Implosion of the HID direct-drive target is accomplished by the generation of a homogeneous, spherical implosion wave capable of isentropically and uniformly compressing the DT fuel to a level of approximately 20 times liquid density. The direct-drive HID target uniformity of power loading requirements are similar to those of the LD direct-drive target: Power loading from the direct drive HID beams[5] must be ±1% uniform in order to permit isentropic compression without Rayleigh-Taylor instabilities. This high uniformity of power loading requirement represents the single most serious HID direct-drive target engineering problem since it involves the simultaneous achievement of equal beam currents together with synchronization of the beams arriving in 4π sterradians. Compared with the indirect drive HID targets described below, the 1% direct drive HID target irradiation requirements are extremely difficult to achieve, thereby making this target design unattractive for HID. Furthermore, having ~100 beam penetrations of the target chamber for the ~100 HID beamlines would cause serious radiation problems for the focusing quadrupole magnets and the downstream components.

4.6.2.2 Heavy Ion Driver Indirect Drive Targets - Although the HID indirect-drive targets are geometrically similar to their LD counterparts (i.e., energy deposition is achieved with two-sided geometries with the HID energy being converted into x-rays within a radiation hohlraum enclosure), there are, in fact, some substantial differences between the LD and HID indirect drive targets.

The design of the HID indirect-drive target is fundamentally different than the LD indirect-drive target design described in Section 4.6.1. According to the HID/target interaction data[1] supplied by the Target Working Group (TWG), the gain of the indirect HID target is more well known and defined than the direct-drive HID target. As a consequence of these data provided by the TWG, the indirect-drive HID target was selected for the baseline. As a further specification of the HID indirect-drive target, two-sided illumination was selected for the Prometheus-H HID baseline design.

Compared with the corresponding LD indirect-drive target, there are substantial differences between the LD and HID indirect-drive targets. Depending upon the plasma atmosphere generated in the LD indirect-drive target, significant numbers of hot electrons can be produced by the laser/plasma interaction; whereas in the case of the HID indirect-drive targets, relatively few hot electrons are produced in the interactions between the decelerating heavy ions and the converter plugs placed at each end of the HID hohlraum. In addition, for the laser-driven hohlraum, the duration of the high intensity portion of the laser pulse is limited by closure of the entrances to the capsule, whereas no comparable effect occurs for the HID hohlraum. This may permit HID indirect-drive targets to outperform LD indirect-drive targets at the same driver energy levels.[6,7]

Selection of parameters for the ID heavy ion target was complicated by the fact that most of the details of such targets are classified. It was known that the targets consist of a fuel capsule surrounded by a radiation case with a high-Z material. The TWG directed the fuel capsule parameters. No details were supplied for the radiation case .

According to TWG guidelines, ". . .*single-sided illumination is still sufficiently speculative that the contractors should continue to carry a two-sided option, . . .*".[8] Based upon this TWG recommendation and information in the open literature[9,10], it was decided to assume two-sided illumination for the Prometheus-H baseline target design.

No guidance was provided on how the DT capsule was to be suspended in the Hohlraum radiation case. A scheme was developed to support the DT fuel capsule with sufficient structural rigidity to tolerate accelerations of 100 g's. Dimensions of the case were chosen for ease of fabrication and ability to withstand the necessary levels of acceleration. The supplied heavy ion ID gain curves indicated energy converter region diameters depending on the ion range and driver energy chosen. The

converter region was determined for the driver design point chosen, allowing some beam misalignment with the target.

References for 4.6

1. Ronald C. Davidson (MIT), et al., "Inertial Confinement Fusion Reactor Design Studies Recommended Guidelines," prepared for DOE Office of Fusion Energy, September 1990.

2. R. L. McCrory, Director, University of Rochester Laboratory for Laser Energetics Annual Report, 23, p. 126, 1984-85.

3. J. J. Thomson, C. E. Max, J. Erkkila, and J. E. Tull, "Laser Light Absorption in Spherical Plasmas," Physical Review Letters 37, pp. 1052-1056 (1976).

4. J. Auerbach, N. C. Holms, J. T. Hunt, and G. J. Linford, "Closure Phenomena in Pinholes Irradiated by Nd:Laser Pulses," Applied Optics 18, 510 (1979).

5. Kessler and von Moellendorff, **Fusion Technology**, 11, 378 (1987).

6. Richard C. Arnold and Rolf W. Mueller, "Parameter Study for Adapting a Heavy-Ion Collider to Drive IFE Ignition Experiments," Theoretische Quantenelektronik, Technische Hochschule, Darmstadt and GSI, Darmstadt, p. 36.

7. R. O. Bangerter, J. W. Mark, and G. Magelssen, "Simple Target Models for Ion Beam Fusion Systems Studies," LLNL Report UCID-20578 (1985).

8. R. Bangerter, et al., "Revised Target Information for IFE Reactor Studies," memo from Roger Bangerter, Chairman TWG, February 1991.

9. R. Bock, "Status and Perspectives of Heavy Ion Inertial Fusion," Gesellschaft fuer Schwerionenforschung mbH, Darmstadt, Germany, GSI-91-13.

10. J. Meyer-ter-Vehn and K. Unterseer, **Laser and Particle Beams**, 3 (3), pp. 283-311.

4.7 Design Rationale for the GIMM

The last and closest optical component in the laser system before the laser light enters the reactor cavity will be subjected to intense transient thermal loading, as well as charged particle and neutron irradiation. For these reasons, it is has been shown in previous laser fusion studies that the engineering design of a long life and reliable last mirror is a major challenge. In this section, the rationale behind the materials selection and design philosophy will be outlined.

Materials Selection - The optical properties of the mirrors surface have been decoupled from the mechanical properties of the supporting structure. In this regard, a great degree of flexibility has been achieved in the design. The surface of the GIMM was chosen to be metallic, because dielectric materials show great sensitivity to the effects of ionizing radiation. The absorption coefficient of MgF_2, and the optical transmission of ZnS degrade by an order of magnitude, after a fluence limit of 10^{16} n/cm^2 accumulates. Even if most of the color centers are annealed out periodically, remaining residual defects would lead to very short lifetime.

The leading high reflectivity candidate metals are aluminum, magnesium, silver, gold, and copper. To select between these metals, the following criteria was considered:

(1) High reflectivity in the wavelength of interest (i.e. 250-500 nm).
(2) Effects of radiation on absorptivity.
(3) Surface temperature rise during the laser pulse.
(4) Thermal fatigue resistance.
(5) Radiation effects on surface deformation.

Although silver has excellent reflectivity, neutron-induced micro-craters are expected to distort the mirror's surface. Near-surface collision cascades in silver will be very dense, because of the high electronic stopping power of silver. On the other hand, copper was excluded on the basis of its high neutron-induced swelling, particularly when it is pure. the higher fatigue strength of aluminum results in a smaller mirror size, when it is compared to magnesium. In addition, the neutron-induced swelling rate of commercial grade aluminum is lower than that of magnesium. For the above reasons, aluminum has been chosen as the material for the surface of the mirror.

The structural support of the mirror is composed of two parts: a low swelling composite SiC high-rigidity component, and a concrete shell for control of thermal deformations. The SiC structure is designed to have small helium cooling channels, running along the length of the mirror. Two other layers are attached immediately underneath. Each one of these two layers is stiffened by I-beams. The SiC composite construction is chosen for the following reasons:

(1) Very low neutron-induced deformations by thermal and irradiation creep mechanisms in the temperature range of 500-700 K.
(2) For porosity of approximately 10-15%, no neutron swelling is to be expected, thus mechanical deformations of the mirror's surface are minimized.
(3) SiC is a low activation material. The choice of SiC will allow passive safety, and shallow land burial of the mirror at the end of life.

In addition to the SiC structure, a concrete shell is designed to provide complete restraint to out-of-plane deformations. This is achieved by sliding bolting mechanisms for the attachment of the bottom of the SiC structure to the concrete shell.

Since the coefficient of thermal expansion of aluminum is higher than that of SiC, a shear graphitic layer is deposited first on the surface of the SiC composite, and the aluminum is added on top of the graphitic shear layer. With this arrangement, in-plane mismatch thermal expansions of the aluminum can be isolated from the SiC composite structure.

More details and design specifics on the GIMM can be found in Section 6.5.1.8, Summary of Laser Driver Subsystems, Grazing Incidence Metal Mirror.